Preprints, 10th IFAC International Symposium on Advances in Automotive Control Columbus, Ohio, USA, August 28-30, 2022

Robust Switching MIMO Control of Turbocharged Lean-Burn Natural Gas Engines

Sree Harsha Rayasam * **Weijin Qiu** * **Gregory M. Shaver** *
Ted Rimstidt ** **Daniel G. Van Alstine** **

* *Purdue University, West Lafayette, IN 47907 USA*
** *Caterpillar Inc., Lafayette, IN 47905 USA*

Abstract: This paper illustrates a multiple-input multiple-output (MIMO) controller design framework and a controller switching algorithm for MIMO controllers to achieve robust coordinated control of turbocharged lean-burn engines. The control problem tracks engine speed, differential pressure across the throttle valve and the air-to-fuel ratio simultaneously to achieve satisfactory engine performance while avoiding compressor surge. The controller design approach is applied to a high-fidelity GT-Power engine model for a lean-burn natural gas engine to assess the closed-loop controller performance. The engine performance with the robust MIMO controller is compared with that using a benchmark production controller to evaluate the additional benefits of the MIMO controller. In a large step increase in desired engine speed and corresponding engine torque, it is observed that the MIMO controller leads to a slightly faster engine speed response. Furthermore, during transience, the minimum air-to-fuel ratio is 20% higher and the peak in differential pressure across the throttle is reduced by 59% when using the MIMO controller.

Keywords: Engine Control, Model-Based Control, Robust MIMO Control, Multivariable Systems, Controller Switching

1. INTRODUCTION

Strict performance requirements, coupled with increasing number of engine architectures to tackle emission regulations require use of effective control design strategies. Engine speed control is of critical importance as deviations from the speed reference leads to an unsatisfactory engine performance. Engine speed control strategies include the classical Proportional-Integral-Derivative (PID) control (Lee et al. (2008)), sliding mode control (SMC) (Chamsai et al. (2015); Li et al. (2017)) and model predictive control (MPC) (Broomhead et al. (2016)). Engine control problems often require multiple parameters to be tracked simultaneously i.e., although the primary control target is engine speed, secondary targets such as air-to-fuel ratio (AFR) and compressor surge margin targets exist which facilitate safe, efficient operation of the engine. Strategies for AFR control include PID control (Ebrahimi et al. (2012)), SMC (Tafreshi et al. (2013); Ebrahimi et al. (2013)). Prevention of compressor surge is an additional challenge for turbocharged engines. The most common method to prevent compressor surge is to open the bypass valve when there is a rapid closure of throttle valve.

All of these control design methods above control a particular output by selecting the most intuitive actuator input among the set of actuators available. However, modern engines are complex, and a significant amount of interaction between controlled outputs and different actuators can exist, as shown in Rayasam et al. (2021). With continuous development of new engine architectures, controller design should be efficient if any additional parameter needs to be controlled. Therefore, control strategies which cover the entire operating range of the engine, are robust and easily tunable while taking into account the multivariate interactions between inputs and outputs are necessary to achieve effective closed-loop performance of the system. In this paper, a framework is developed to design robust MIMO controllers for lean-burn natural gas variable speed engines that can achieve coordinated control of the desired controlled outputs while considering actuator limitations and model uncertainties.

Furthermore, controller switching algorithms are of practical importance as more than one controller is generally required to achieve satisfactory control over the entire operating space of many physical systems. Gain scheduling, interpolation of controllers, fuzzy-logic are popular switching methods but they do not guarantee robustness. A controller switching algorithm developed in Cheong and Safonov (2011), which uses slow-fast controller decomposition is extended in this paper such that it can be applied to scaled MIMO controllers in their state-space form.

The rest of the paper is organized as follows: Section 2 introduces the control problem and the model used for controller synthesis. Section 3 describes the controller synthesis and controller switching algorithms. Simulation results using the controller developed by this framework are

⋆ The effort was funded by Caterpillar Inc.

discussed in Section 4. Section 5 contains the conclusions of this paper.

2. CONTROL PROBLEM FORMULATION AND STATE-SPACE MODEL

The engine in consideration is a turbo-charged spark-ignited engine equipped with four actuators: throttle valve, fuel valve, bypass valve and an active wastegate valve used in an off-road application. Fig. 1 depicts the engine architecture.

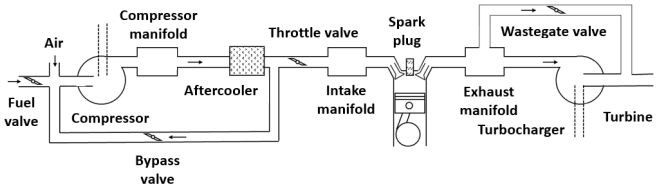

Fig. 1. Engine architecture

The control-oriented model consist of five states: engine speed, intake manifold pressure, compressor manifold pressure, exhaust manifold pressure, turbocharger speed; four inputs: throttle valve effective area, bypass valve effective area, fuel flow rate, wastegate valve effective area; one disturbance due to load torque acting on the engine; three outputs: engine speed, differential pressure across the throttle valve (as a means to prevent compressor surge) and AFR (to restrict engine emissions). Table. 1 summarizes the definition of these control-oriented model variables along with their units.

Table 1. Control-oriented model variables

Variable	Description	Unit
State (x_1)	Engine speed	rad/s
State (x_2)	Intake manifold pressure	Pa
State (x_3)	Compressor manifold pressure	Pa
State (x_4)	Exhaust manifold pressure	Pa
State (x_5)	Turbocharger speed	rad/s
Input (u_1)	Effective throttle area	sq.m
Input (u_2)	Effective bypass area	sq.m
Input (u_3)	Fuel flow rate	kg/s
Input (u_4)	Effective wastegate area	sq.m
Disturbance (u_d)	Load torque	Nm
Output (y_1)	Engine speed	rad/s
Output (y_2)	Differential pressure across the throttle valve	Pa
Output (y_3)	AFR	-

Using laws of conservation of mass and energy, the control-oriented nonlinear model for the engine can be represented as follows:

$$
\begin{aligned}
\dot{x}_1 &= \frac{1}{I_{eng}}\Big(\frac{\eta_v \eta_{thermal} Q_{LHV} V_D u_3}{4\pi R T_{im} W_{cyl}} x_2 - u_d\Big) \\
\dot{x}_2 &= \frac{T_{im} R}{V_{im}}\big(W_{thr} - W_{cyl}\big) \\
\dot{x}_3 &= \frac{T_{bm} R}{V_{bm}}\big(W_{comp} - W_{thr} - W_{byp}\big) \\
\dot{x}_4 &= \frac{T_{em} R}{V_{em}}\big(W_{cyl} - W_{turb} - W_{wg}\big) \\
\dot{x}_5 &= \frac{1}{I_{turbo}}\Big(\frac{P_{turb} - P_{comp}}{x_5} - \tau_{loss}\Big) \\
y_1 &= x_1 \\
y_2 &= x_3 - x_2 \\
y_3 &= \frac{W_{cyl} - u_3}{u_3}
\end{aligned}
\tag{1}
$$

Table 2. Definition of terms in the nonlinear model

Variable	Description
I_{eng}	Engine shaft inertia
I_{turbo}	Turbocharger shaft inertia
η_v	Volumetric efficiency
$\eta_{thermal}$	Brake thermal efficiency
Q_{LHV}	Lower heating value of the fuel
V_D	Displacement volume
R	Gas constant
T_{im}	Intake manifold temperature
T_{bm}	Compressor manifold temperature
T_{em}	Exhaust manifold temperature
V_{im}	Intake manifold volume
V_{bm}	Compressor manifold volume
V_{em}	Exhaust manifold volume
W_{thr}	Throttle valve mass flow
W_{byp}	Bypass valve mass flow
W_{wg}	Wastegate valve mass flow
W_{cyl}	Cylinder mass flow
W_{comp}	Compressor mass flow
W_{turb}	Turbine mass flow
P_{comp}	Compressor power
P_{turb}	Turbine power
τ_{loss}	Turbocharger shaft frictional torque

The nonlinear model in (1) is then linearized around different equilibrium points to obtain a linear model which can be expressed in the standard state-space form as shown in (2).

$$
\begin{aligned}
\dot{x} &= A_i \delta x + B_i \delta u + F_i \delta u_d \\
\delta y &= C_i \delta x + D_i \delta u
\end{aligned}
\tag{2}
$$

where x are model states, y are controlled outputs, u are control inputs, u_d is the disturbance. The subscript i is the index of the sub-model which is selected based on the current operating region of the model. For detailed derivations and explicit expressions of all the terms in the nonlinear model and the equilibrium points used to linearize the nonlinear model, please refer to Rayasam et al. (2021).

For the purpose of controller synthesis, the linear state-space model is normalized using diagonal scaling matrices: N_x, N_u, N_y, N_{u_d}. The elements in these matrices are obtained by estimating the maximum amount of change in the corresponding variable for the operating region of

interest. The scaled matrices (denoted by bar) and original matrices are related per (3).

$$\bar{A} = {N_x}^{-1} A N_x \quad \bar{B} = {N_x}^{-1} B N_u \quad \bar{F} = {N_x}^{-1} F N_{u_d}$$
$$\bar{C} = {N_y}^{-1} C N_x \quad \bar{D} = {N_y}^{-1} D N_u \tag{3}$$

3. CONTROLLER SYNTHESIS AND CONTROLLER SWITCHING

3.1 Control Configuration

The robust control configuration for the control problem is shown in Fig. 2. The weighted target performances, z_p include the weighted forms of engine speed error, throttle differential pressure error and AFR error. The weighted actuator performances, z_u include the weighted forms of throttle valve effective area, bypass valve effective area, fuel flow rate and wastegate valve effective area. z_p and z_u together form the exogenous output vector. Since the weighted target performances are obtained by multiplying the closed-loop error by a performance weight W_p, W_p penalizes any non-zero tracking error. In other words, W_p is used to define the required closed-loop tracking performance of the controlled outputs as a function of frequency. Similarly, since weighted actuator performances are the weighted forms of control efforts, actuator weight W_u penalizes undesired actuator usage. W_u is a frequency dependent design parameter which is selected based on actuator limitations. The three references for the controlled outputs as well the disturbance load torque act as the exogenous inputs to the control system. To account for any model inaccuracies, a frequency dependent uncertainty is considered and $x\Delta$, $y\Delta$, $u\Delta$ denote the state, output and input perturbations respectively. Controlled inputs are the variables the controller can manipulate and these include the throttle valve effective area, bypass valve effective area, fuel mass flow rate and wastegate valve effective area. The core idea behind robust MIMO controller design is to minimize the gain between exogenous inputs and exogenous outputs in the presence of model uncertainties using all the available controlled inputs. A more detailed control block diagram that represents the relationship between exogenous outputs and exogenous inputs is shown in Fig. 3. The transfer functions in Fig. 3, G_x and G_d can be calculated from the linear model and are $\left(sI - \bar{A}\right)^{-1}\bar{B}$ and $\left(sI - \bar{A}\right)^{-1}\bar{F}$, respectively.

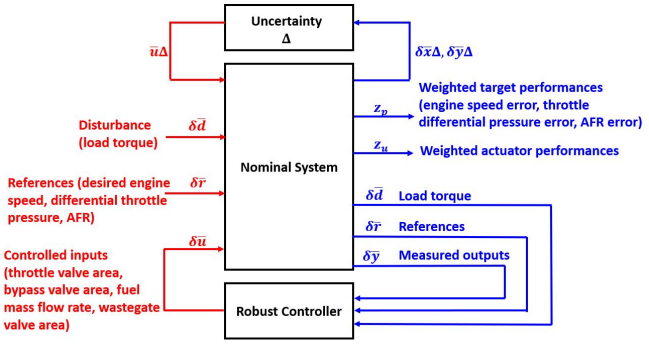

Fig. 2. Robust control configuration

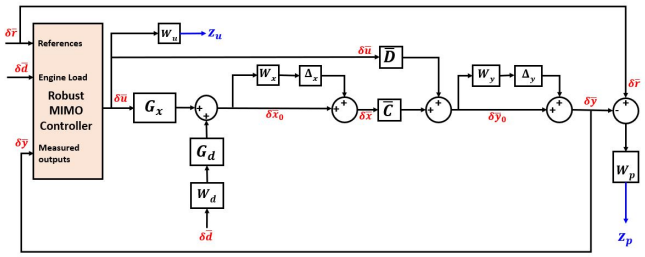

Fig. 3. Detailed control block diagram for controller design

Table 3. W_p parameters

Controlled output	Parameter	K_1	K_2	K_3	K_4
y_1	ω^*_B	0.1	0.2	0.36	0.5
	A	0.01	0.5	0.13	0.2
	M	3	5	5	5
y_2	ω^*_B	0.1	0.2	0.36	0.5
	A	0.01	0.5	0.13	0.2
	M	3	5	5	5
y_3	ω^*_B	1.5	2.5	1	0.1
	A	0.01	0.5	0.5	0.1
	M	2	5	5	10

Mathematically, the exogenous output vector $z = \begin{bmatrix} z_p \\ z_u \end{bmatrix} = \begin{bmatrix} W_p e \\ W_u u \end{bmatrix}$. Therefore, the shape of performance weights and actuator weights determine the closed-loop tracking performance and actuator responses. A first-order performance weight of the form shown in (4) is chosen for all three controlled outputs across all operating points to synthesize four robust MIMO controllers. This choice penalizes tracking error at low frequencies (including steady-state) while reducing the penalty at higher frequencies.

$$W_p = \frac{\frac{s}{M} + {\omega^*}_B}{s + {\omega^*}_B A} \tag{4}$$

The parameters of the performance weights used for controller design are listed in Table 3 and the closed-loop response of the controlled outputs can be tuned with these parameters.

To prevent undesired actuator usage, W_u is modeled as per (5), thus allowing actuator usage at low frequencies while penalizing it at higher frequencies.

$$W_{u,throttle} = \frac{\frac{s}{50} + 1}{\frac{s}{5000} + 1} \qquad W_{u,bypass} = \frac{\frac{s}{40} + 1}{\frac{s}{4000} + 1}$$
$$W_{u,fuel} = \frac{\frac{s}{30} + 1}{\frac{s}{3000} + 1} \qquad W_{u,wastegate} = \frac{\frac{s}{10} + 1}{\frac{s}{1000} + 1} \tag{5}$$

Modeling errors and errors arising from plant linearization are approximated by considering multiplicative uncertainty of both states and outputs. The uncertainty matrices are expressed as diagonal matrices, each element in the matrix takes the form:

$$w_i = \frac{s/\omega + r_0}{s/(r_\infty \omega) + 1} \tag{6}$$

where r_0 is the relative uncertainty at steady-state, ω is the approximate frequency where uncertainty reaches 100%. r_∞ is estimated to be $2r_0$.

Uncertainty of the plant states at steady-state is estimated as follows: $r_0 = max\left(\frac{\delta x_{GT,i} - \delta x_{linear,i}}{\delta x_{GT,i}}\right)$, $x_{GT,i}$ denotes the i^{th} state estimated by the truth-reference GT-Power model, $x_{linear,i}$ denotes the corresponding state estimated by the linear model used for controller synthesis. Among the outputs, only AFR (y_3) is considered uncertain since the first two outputs (engine speed, $y_1 = x_1$ and differential pressure across the throttle, $y_2 = x_3 - x_2$) can be expressed as a linear combination of states. On the other hand, (y_3) is calculated by $\frac{W_{cyl} - u_3}{u_3}$ cannot directly be expressed in a linear form using states, inputs and needs to be linearized, which results in loss of accuracy. Hence, to avoid over estimating the model uncertainty and thereby synthesizing an unnecessarily conservative robust controller, y_1 and y_2 are not considered uncertain. The perturbed states, outputs (as seen in Fig. 3) are defined as: $\delta\bar{x} = \delta\bar{x}_0\,(1 + W_x\Delta_x)$ and $\delta\bar{y} = \delta\bar{y}_0\,(1 + W_y\Delta_y)$, where $\delta\bar{x}_0$ and $\delta\bar{y}_0$ are the nominal state and output vector respectively, W_x is a diagonal matrix whose elements are defined according to (6). $\Delta_x = \text{diag}\{\delta x_1, \delta x_2, \delta x_3, \delta x_4, \delta x_5\}$ is a diagonal matrix where each entry in the matrix, $\delta x_i, i = 1, 2, 3, 4, 5 \in [-1, 1]$. Similarly, W_y is a diagonal matrix as well, whose elements are defined according to (6). Since only AFR is considered uncertain, $\Delta_y = \text{diag}\{0, 0, \delta y_3\}$ with $\delta y_3 \in [-1, 1]$.

Robust control theory described in Skogestad and Postlethwaite (2007) derives that robust stability and robust performance for a closed-loop system are guaranteed if the following inequality is true:

$$\sup_{\omega \in \mathcal{R}} \mu_\Delta[M(P, K)(j\omega)] < 1$$

where $M(P, K)$ is the closed-loop transfer function matrix from exogenous inputs to exogenous outputs for an uncertain plant P and controller K, μ is called the structured singular value of the closed-loop system.

To synthesize the controller K which satisfies the above condition, μ-synthesis method using D-K iteration is utilized. MATLAB's D-K iteration is an optimization algorithm that iteratively solves for a controller K until the robustness condition is satisfied for a given plant and uncertainty model. In cases where the algorithm cannot synthesize a controller that satisfies the robustness requirement i.e. when $\mu > 1$, performance weights need to be tuned to relax the closed-loop performance criteria. Table 4 lists the values of μ for each controller designed and the corresponding operating region. Since $\mu < 1$ for all controllers, it can be said that the system is robust for the estimated uncertainty, performance criteria and actuator limitations.

Table 4. Controller operating regions

Controller	μ	Operating region [RPM]
K_1	0.96	600 - 1000
K_2	0.92	1000 - 1200
K_3	0.98	1200 - 1550
K_4	0.82	1550 - 1800

3.2 Controller Switching Methodology

To enable smooth switching between multiple controllers, each MIMO controller K_i is decomposed into two parts, a "slow" part ($K_{i,s}$) and a "fast" part ($K_{i,f}$) such that $K_i = K_{i,s} + K_{i,f}$, and the poles of $K_{i,s}$ are slower than the poles of $K_{i,f}$. Both $K_{i,s}$ and $K_{i,f}$ are expressed in their standard state-space form as shown in (7).

$$\begin{aligned} \dot{x}_{i,s} &= A_{i,s}x_{i,s} + B_{i,s}z_{i,s} \quad y_{K_{i,s}} = C_{i,s}x_{i,s} + D_{i,s}z_{i,s} \\ \dot{x}_{i,f} &= A_{i,f}x_{i,f} + B_{i,f}z_{i,f} \quad y_{K_{i,f}} = C_{i,f}x_{i,f} + D_{i,f}z_{i,f} \end{aligned} \tag{7}$$

where $x_{i,s}$, $y_{K_{i,s}}$, $z_{i,s}$ represent the states, outputs, inputs of $K_{i,s}$ respectively, and $x_{i,f}$, $y_{K_{i,f}}$, $z_{i,f}$ represent the states, outputs, inputs of $K_{i,f}$ respectively.

A smooth transition of control authority from K_i to K_j at the switching instant, t_s can be achieved by performing state-reset of both slow and fast controllers as follows:

$$\begin{aligned} &x_{j,f}(t_s^+) = 0 \\ &x_{j,s}(t_s^+) = C_{j,s}^{\dagger} N_{j,u}^{-1}\{u(t_s^-) - u_{j,e} - N_{j,u}\,(D_{j,s} + D_{j,f})\,z(t_s^-)\} \end{aligned} \tag{8}$$

where $N_{j,u}$ is the input scaling matrix, $\dagger$ stands for the pseudo-inverse of a matrix, $u_{j,e}$ is the equilibrium control input vector of the linear plant corresponding to controller K_j, z is the input vector to controller K_j.

4. SIMULATION RESULTS AND ANALYSIS

The operating space of the engine is between 600 RPM and 1800 RPM. In the test discussed in this paper, the desired engine speed is changed from 600 RPM (Idle) to 1800 RPM (Mode 1 - corresponding to 100% power) with load torque varying as shown in Fig. 4. Since the engine operating space is between 600 RPM and 1800 RPM, this test is also the largest step increase in engine speed possible for the engine. Among the three references (engine speed, differential throttle pressure, AFR), desired engine speed is an independent target while the desired values of differential pressure across the throttle valve and AFR are obtained using maps dependent on actual engine speed and load fraction. These maps are not plotted in this paper.

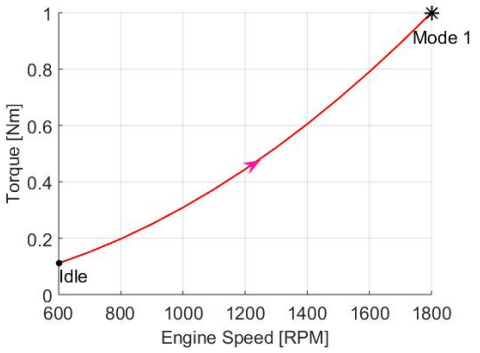

Fig. 4. Load torque profile

Brief Description of the Benchmark Controller

In the benchmark production controller for this application, the throttle valve controller regulates engine speed

by measuring speed tracking error as the feedback. Based on the inlet flow to the engine, the fuel flow controller manipulates fuel quantity to satisfy AFR limits. The bypass valve controller is tuned to actuate the bypass valve to track the differential pressure across the throttle valve during transient phase of engine operation. Similarly, the wastegate valve controller is tuned to actuate the wastegate valve to track the differential pressure across the throttle valve at close to steady-state operation. Therefore, it is a decentralized controller where a specific actuator input is chosen to track a specific controlled output. The robust model-based MIMO control strategy developed in this paper is significantly different where all four actuators are commanded in a coordinated fashion to track the engine speed, differential pressure across the throttle and AFR simultaneously with no specific input-output pairing. In the results that follow, 'SISO PID' stands for the benchmark controller and 'Robust MIMO' stands for the robust MIMO controller designed in this paper. Also, engine torque, power, fuel flow rates are normalized with respect to their rated values.

In Fig. 5, it is observed that engine speed response is faster with the MIMO controller but has an overshoot in the response. Both controllers take similar amount of time (13 s) to settle at 1800 RPM. A better AFR response is obtained with the MIMO controller, both during transient and steady-state. Soon after the target engine speed is set to 1800 RPM, a dip in AFR reaching approximately 12 is observed with the benchmark controller, while it only drops to 15 with the MIMO controller i.e. the minimum AFR during transience is 20% higher with the MIMO controller. At steady-state, tighter AFR control is achieved with the MIMO controller. The transient fuel flow commands are slightly different during transient, leading to a different engine speed response, while the steady-state fuel flow commands are the same in both controllers. In Fig. 6, it is seen that throttle valve is saturated, fully open for a few seconds during the transient phase, in both cases. However, as the throttle valve starts to close at 27 s, throttle valve position in the benchmark controller reaches 0.4, exhibits a more aggressive behavior while the MIMO controller reaches only 0.6 and has a gentler response. The steady-state throttle valve position in both cases is approximately 0.63. The wastegate valve position at steady-state for the benchmark controller is 0.55 while it is 0.45 for the MIMO controller. MIMO controller commands the bypass valve to open slightly (position = 0.05) at steady-state, while the benchmark controller shuts it completely. A significantly better transient differential throttle pressure tracking is achieved with the robust MIMO controller. During transient, differential throttle pressure reaches 97 kPa for the benchmark controller, while it is only as high as 39 kPa for the MIMO controller i.e. the peak value of differential throttle pressure is 59.7% lower when using the MIMO controller. Although the steady-state value of differential throttle pressure is 35 kPa in both cases, the MIMO controller is able to control the output at its desired value much faster (Benchmark reaches steady-state at 43 s, MIMO reaches steady-state at 30 s). It can also be noticed that a smoother steady-state response is attained with the MIMO controller. Fig. 7 shows the compressor operation map for this simulation and it can be observed that compressor operates within the boundary in both cases. However, the benchmark controller operates the compressor closer to the surge boundary while the MIMO controller operates it farther away from the surge boundary.

5. CONCLUSIONS

This paper outlines a framework to synthesize robust $\mathcal{H}_\infty$ controllers using the μ-synthesis algorithm. A controller switching algorithm that uses slow-fast controller decomposition, state-reset is developed to switch between multiple MIMO controllers. This entire framework is applied to a high-fidelity GT-Power model of a turbocharged natural gas SI engine to demonstrate the closed-loop performance of the switching robust MIMO controller and the results obtained are compared with those obtained with the benchmark controller. In a large step increase in desired engine speed and corresponding engine torque, it is observed that the MIMO controller leads to a slightly faster engine speed response. In addition, minimum AFR is 20% higher and the peak in differential pressure across the throttle is reduced by 59% during transience when the MIMO controller is used.

ACKNOWLEDGEMENTS

This effort was funded by Caterpillar Inc.

REFERENCES

Broomhead, T., Manzie, C., Hield, P., Shekhar, R., and Brear, M. (2016). Economic model predictive control and applications for diesel generators. *IEEE Transactions on Control Systems Technology*, 25(2), 388–400.

Chamsai, T., Jirawattana, P., and Radpukdee, T. (2015). Robust adaptive PID controller for a class of uncertain nonlinear systems: an application for speed tracking control of an SI engine. *Mathematical Problems in Engineering*, 2015.

Cheong, S.Y. and Safonov, M.G. (2011). Slow-fast controller decomposition bumpless transfer for adaptive switching control. *IEEE transactions on automatic control*, 57(3), 721–726.

Ebrahimi, B., Tafreshi, R., Masudi, H., Franchek, M.A., Mohammadpour, J., and Grigoriadis, K. (2012). A systematic air-fuel ratio control strategy for lean-burn SI engines. *IFAC Proceedings Volumes*, 45(30), 296–301.

Ebrahimi, B., Tafreshi, R., Mohammadpour, J., Franchek, M., Grigoriadis, K., and Masudi, H. (2013). Second-order sliding mode strategy for air–fuel ratio control of lean-burn SI engines. *IEEE Transactions on Control Systems Technology*, 22(4), 1374–1384.

Lee, S., Yim, J., Lee, J., and Sul, S. (2008). Design of speed control loop of a variable speed diesel engine generator by electric governor. In *2008 IEEE Industry Applications Society Annual Meeting*, 1–5.

Li, X., Ahmed, Q., and Rizzoni, G. (2017). Nonlinear robust control of marine diesel engine. *Journal of Marine Engineering & Technology*, 16(1), 1–10.

Rayasam, S.H., Qiu, W., Rimstidt, T., Shaver, G.M., Van Alstine, D.G., and Graziano, M. (2021). Control-oriented modeling, validation, and interaction analysis of turbocharged lean-burn natural gas variable speed engine. *International Journal of Engine Research*, 14680874211064210.

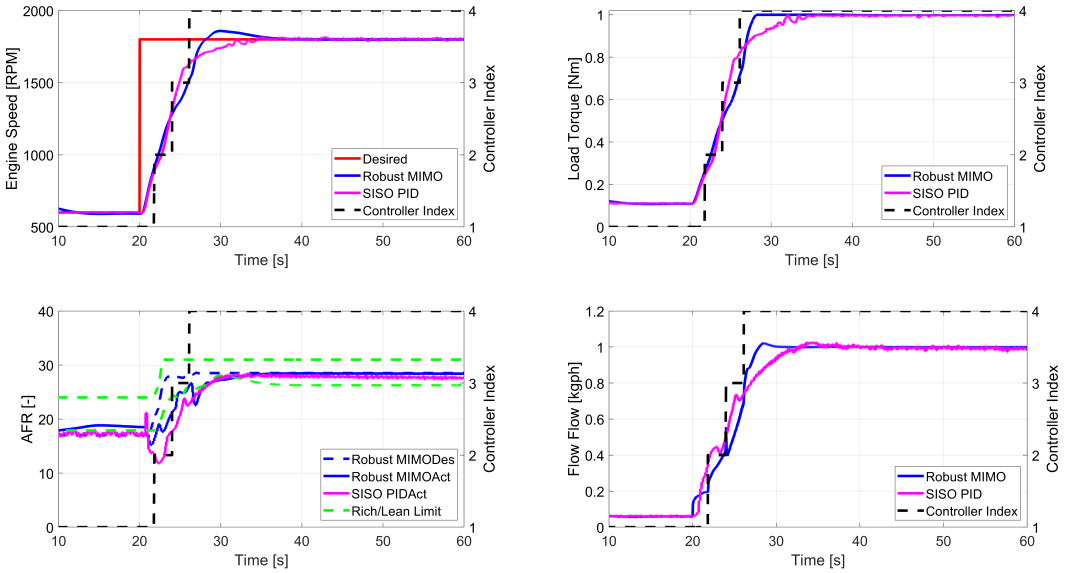

Fig. 5. Top: Engine speed, load torque; Bottom: AFR, fuel flow rate

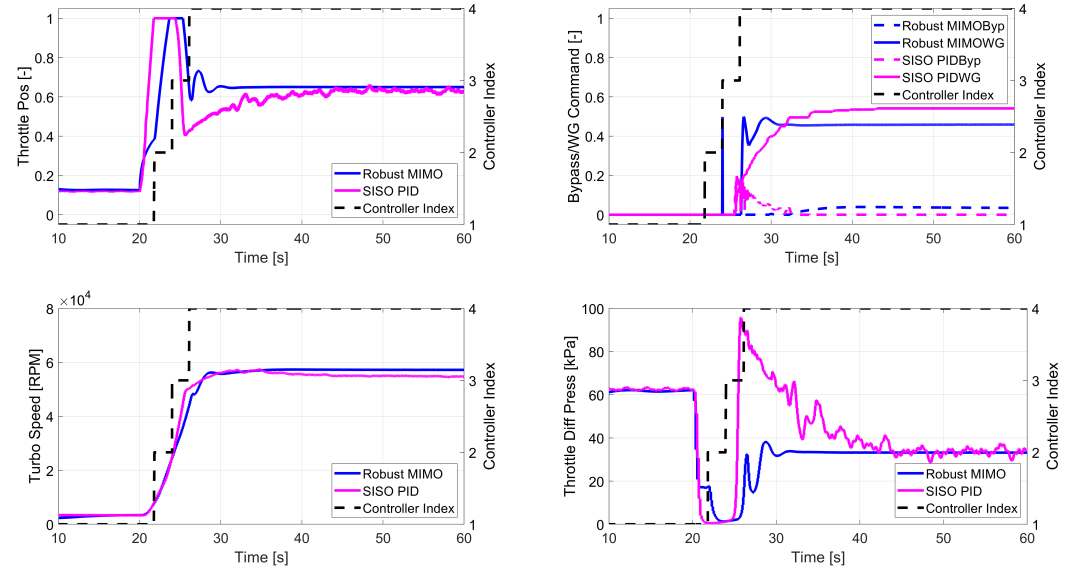

Fig. 6. Top: Throttle position, Bypass/Wastegate position; Bottom: Turbocharger speed, Throttle differential pressure

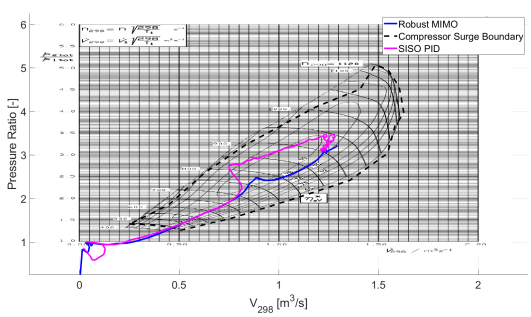

Fig. 7. Compressor operation

Skogestad, S. and Postlethwaite, I. (2007). *Multivariable feedback control: analysis and design*, volume 2. Wiley New York.

Tafreshi, R., Ebrahimi, B., Mohammadpour, J., Franchek, M.A., Grigoriadis, K., and Masudi, H. (2013). Linear dynamic parameter-varying sliding manifold for air–fuel ratio control in lean-burn engines. *IET Control Theory & Applications*, 7(10), 1319–1329.